International Journal of Modern Engineering Research (IJMER)
www.ijmer.com Vol.3, Issue.2, March-April. 2013 pp-1041-1055 ISSN: 2249-6645

Reduction of Noise Effect in Land-Buried Target Shape Recognition through Polari Metric GPR Images

Khalid M. Ibrahim, [1]Khalid F. A. Hussein, [2]Abd-El-Hadi A. Ammar[3]
[1]*Assoc. ResearchersMicrowave Engineering Dept., Electronics Research Inst., Cairo, Egypt*
[2]*Assoc.Prof. Microwave Engineering Dept., Electronics Research Inst., Cairo, Egypt*
[3]*Prof. Electronics and Electrical Communications Dept., Faculty of engineering, El-AZHAR University, Cairo, Egypt*

Abstract:*A new treatment of the buried object shape retrieval and target recognition from noisy polarimetric GPR images is introduced. The construction of GPR system proposed for obtaining high resolution polarimetrictwo-dimensional cross-range images of objects buried under the surface of a ground soil is described. A granular noise filter (GNF) is introduced to get an image with increased signal-to-noise ratio (SNR). An algorithm to extract a two-dimensional shape of the buried object is introduced. A shape smoothing filter (SSF) is then applied for further elimination of the errors resulting due to granular noise effect on the two-dimensional shape retrieval process. A shape recognition algorithm is applied to compare the retrieved shape for the buried object to a reference target shape to take a match or mismatch decision. The proposed GPR antenna system and the suggested algorithms for noise reduction, shape extraction and target recognition are examined through FDTD simulation. The numerically obtained results show that proposed noise reduction technique with the proposed GPR system and the suggested algorithms for shape extraction and target shape recognition are efficient and successful in all the examined cases.*

I. INTRODUCTION

The imaging of the ground subsurface is becoming more important for land mine detection and archaeological investigations. It is important to obtain an image of the subsurface to find out the position of buried objects and the composition of the subsurface. This information is preferably obtained without disrupting the subsurface, and the technique dedicated to this task is called a non-destructive technique, to which category the imaging GPR belongs. Many GPR imaging systems have been proposed in the literature [1–9]. Although good depth resolution can usually be realized in GPR images using frequency diversity, good resolution in the cross-range dimensions is much harder to achieve [10].The present work introduces a new polarimetric GPR imaging system to obtain two-dimensional image for the buried objects causing in homogeneity in the ground soil. This imaging GPR system was partially described in [11].

The noise added at the receiver of a GPR system results in distortion of the GPR image that may disturb the process of image construction and hence may lead to an erroneous decision during the process of buried target recognition and, thereby, leading to false alarms or missed target detections. To make the GPR data more reliable for retrieving the correct information for the ground subsurface, a number of filtering techniques have been proposed to enhance the SNR of the data [1].

The present work introduces a new technique to reduce the effect of white Gaussian noise in a polarimetric GPR system that uses four polarization channels to obtain four high resolutiontwo-dimensional images in the cross-range for the objects buried in the ground soil. Two of the obtained images represent the complex scattering parameters from co-polarization channels (*xx* and *yy*) whereas the other images represent the complex scattering parameters from cross-polarization channels (*xy* and *yx*). A Granular Noise Filter (GNF) and a Smoothed Shape Filter (SSF) are applied to enhance the SNR of the GPR image and hence leading to a more reliable target recognition process.

The paper introduces mathematical and numerical algorithms for extracting the buried object shape and recognizing the shape of a reference target and to show the effect of the SNR on the target shape recognition process. Numerical results are presented to demonstrate the efficiency of the proposed noise reduction techniques and the imaging GPR system together with the developed mathematical and numerical techniques.

II. CONSTRUCTION AND PRINCIPLE OF OPERATION OF THE IMAGING GPR SYSTEM

The antenna system of the GPR is constructed as a clustered two-dimensional planar array of coplanar crossed-dipole antennas. This array can be viewed as two-dimensional array of $K \times K$ rectangular clusters; each cluster can be considered as a sub-array of $M \times N$ crossed-dipole elements. A cluster composed of 7×7 elements is shown in Figure 1a. The element of a cluster, or sub-array, is composed of an *x*-oriented dipole crossed with another *y*-oriented dipole. All the elements of a cluster act as receiving antennas except for the central one which is housed in a conducting reflector and acts as a transmitter for illuminating the rectangular area just below the corresponding cluster of the antenna array. As shown in Figure1b, the conducting housing over the transmitting crossed-dipole is a partial cover made to prevent direct coupling between the transmitting antenna and all the receiving antennas.

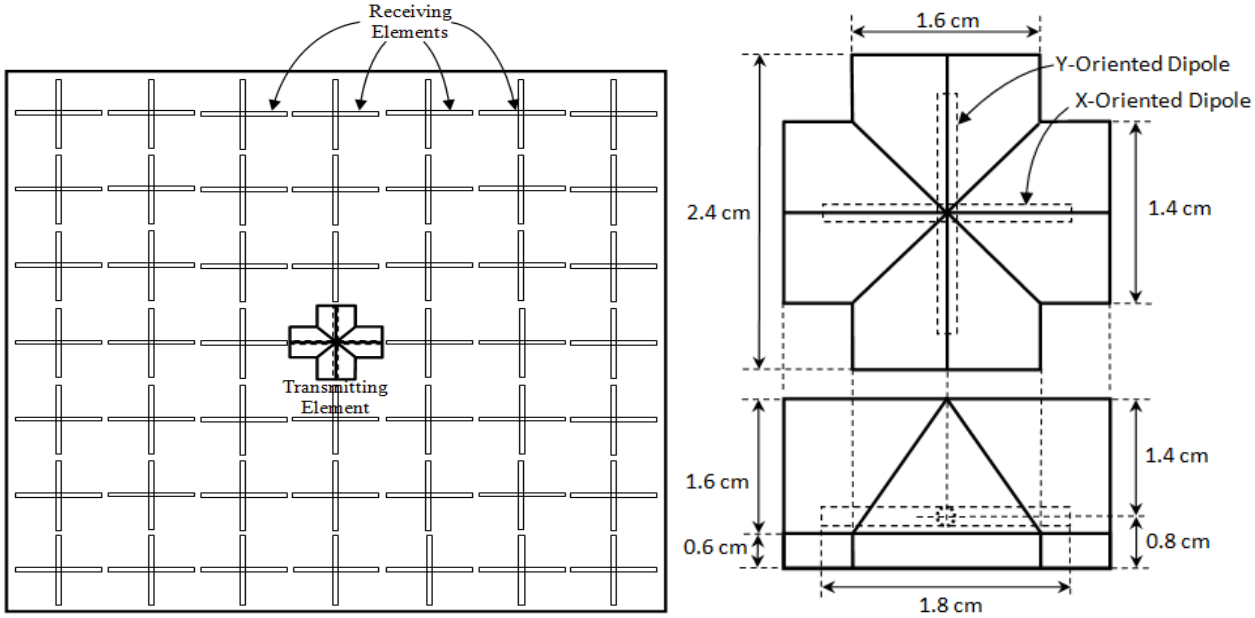

(a) GPR antenna system (b) Transmitting antenna

Figure 1: GPR antenna system composed of 7×7 antenna elements; the central element is a transmitting crossed-dipole partially enclosed inside a metallic reflector and the remaining elements are receiving crossed dipole antennas.

Let the GPR antenna system consist of a reflector housed horizontal (parallel to the ground surface) dipole antenna for illuminating the soil. Let an array of similar receiving dipole antenna elements be arranged in rows and columns so as to get two dimensional images for inhomogeneous bodies underlying the ground surface. The transmitting dipole antenna is housed in metallic reflector to prevent direct coupling between the transmitting antenna and all receiving antennas. When the sensor is placed over empty ground, the coupling between the transmitting antenna '1' and a receiving antenna '2', $|S_{21}|$, is very small. As the sensor is placed over a soil with an object buried near enough to the ground surface, the inhomogeneity occurring due to the difference between the electromagnetic properties of the soil and that of the buried object leads to scatter a portion of the signal radiated by the transmitting antenna to the receiving antenna and, thereby, increasing the coupling between the transmitting and receiving antennas. Thus, the increase in the electromagnetic coupling can be used to indicate the presence of an in homogeneity just below the receiving dipole. If an enough number of closely spaced receiving elements which are regularly arranged in the plane just above the ground surface, a two dimensional image can be constructed from the scattering parameter data between transmitting and receiving antenna elements. This can be explained in view of the FDTD simulation results presented in Figure2. The electric field distribution in an empty soil due to the radiation from the *x*-oriented transmitting dipole is presented in Figure2a. The electric field at the ground surface is very weak and hence the signal arriving at an *x*-oriented receiving antenna element is almost zero. When a metallic block is buried in the soil near the ground surface, the electric field launched into the soil by the transmitting dipole is guided between the upper face of the metallic block and the ground surface, as shown in Figure2b and, thereby, arriving at the receiving dipoles. Thus the existence of the metallic block leads to increase the coupling between the transmitting dipole and those receiving dipoles lying just above the buried block. Similarly, the coupling between a *y*-oriented transmitting dipole and *y*-oriented receiving dipoles is considerably increased due the existence of a buried metallic block. This can be shown by comparing between Figures 2c and 2d.

For the soil types that result in changing the polarization of the propagating wave due the rotation of the electric field vector about the direction of propagation, the data obtained from the four polarimetric channels are required to get the complete GPR image. For the other types of the soils the data obtained from the co-polarization channels (*xx* and *yy*) are enough to get the complete two-dimensional image for the ground subsurface.

The complete GPR operation including polarimetric imaging, granular noise filter, buried object shape retrieval, and target shape recognition is described by the block diagram presented in Figure 3. The detailed explanations of the processes involved in this block diagram are provided by the following sections.

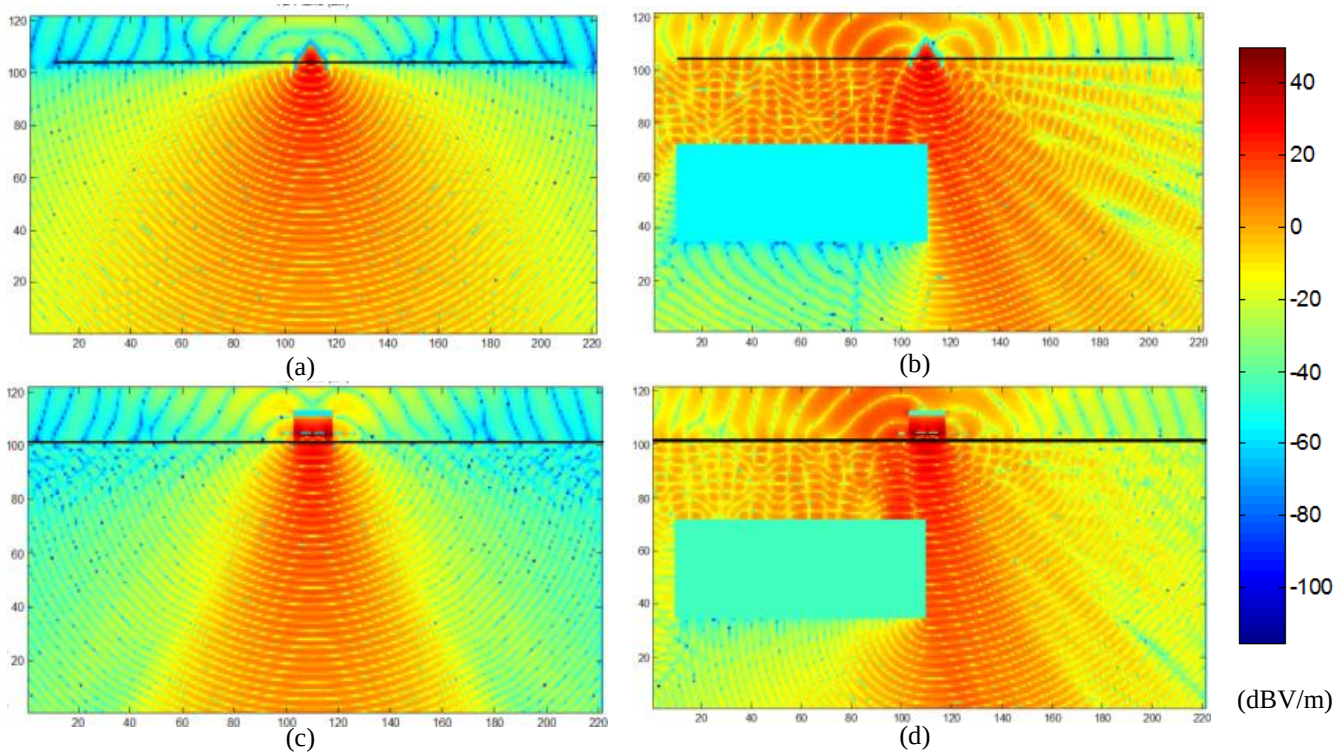

Figure2: Distribution of the electric field in the longitudinal section (*yz*-plane) of the soil when:(a) the soil is empty and the transmitting *x*-oriented dipole is activated, (b) a rectangular box-shaped block is buried at a depth of 10 cm below the ground surface and the transmitting *x*-directed dipole is activated, (c) the soil is empty and the transmitting *y*-oriented dipole is activated, and (d) a rectangular box-shaped block is buried at a depth of 10 cm below the ground surface and the transmitting *y*-directed dipole is activated

III. TWO-DIMENSIONAL IMAGE CONSTRUCTION

AGPR image for the inhomogeneous bodies buried below the ground surface is constructed through four polarimetric channels. For explaining the imaging method, we can take the *xy*-channel as an example. The scattering parameters from the *xy*-channel are obtained by activating only the *y*-oriented transmitting dipole elements at the center of each cluster without activating the *x*-oriented transmitting elements. Under this situation, the received signals at the *x*-oriented dipole elements of a specific sub-array are divided by the signal applied to the central *y*-oriented transmitting dipole for each cluster of the GPR array to obtain the corresponding scattering parameters. Thus, the resulting *xy*-channel images are actually the complex scattering parameters representing the electromagnetic coupling between each of the *x*-oriented receiving dipoles and the *y*-oriented transmitting dipole at the center of the same cluster of the receiving dipoles. By gathering the data obtained from each cluster of the GPR array, the complete *xy*-channel image is obtained.

The four-channel two-dimensional complex polarimetric images for the buried object can be constructed by the following four matrices obtained from each cluster of the antenna array:

$$S_{k,l}^{xx} = \left[S_{k,l,m,n}^{xx}\right], k = 1,2,..,K; l = 1,2,..,K; m = 1,2,..,M;\ n = 1,2,..,N \quad (1)$$

$$S_{k,l}^{xy} = \left[S_{k,l,m,n}^{xy}\right], k = 1,2,..,K; l = 1,2,..,K; m = 1,2,..,M;\ n = 1,2,..,N \quad (2)$$

$$S_{k,l}^{yx} = \left[S_{k,l,m,n}^{yx}\right], k = 1,2,..,K; l = 1,2,..,K; m = 1,2,..,M; n = 1,2,..,N \quad (3)$$

$$S_{k,l}^{yy} = \left[S_{k,l,m,n}^{yy}\right], k = 1,2,..,K; l = 1,2,..,K; m = 1,2,..,M;\ n = 1,2,..,N \quad (4)$$

Where$K$is the number of clusters, constituting the GPR antenna array; M and N are the numbers of rows and columns, respectively, of the receiving antenna elements in each cluster.

For each of the four polarimetric channels, the complete image is constructed from the $K \times K$ clusters; for example to the complete *xx*-channel image is constructed as follows

$$S^{xx} = \begin{bmatrix} \left[S_{1,1,m,n}^{xx}\right]\left[S_{1,2,m,n}^{xx}\right] & \cdots & \left[S_{1,K,m,n}^{xx}\right] \\ \left[S_{2,1,m,n}^{xx}\right]\left[S_{2,2,m,n}^{xx}\right] & & \left[S_{2,K,m,n}^{xx}\right] \\ \vdots & \ddots & \vdots \\ \left[S_{K,1,m,n}^{xx}\right]\left[S_{K,2,m,n}^{xx}\right] & \cdots & \left[S_{K,K,m,n}^{xx}\right] \end{bmatrix}, m = 1,2,..,M;\ n = 1,2,..,N \quad (5)$$

The other three images for the other three polarization channels are similarly constructed. In this way, eight real visualized images can be constructed from the polarimetric GPR data using a proper numerically scaled color maps for displaying the following eight sets of two-dimensional data:$\mathrm{Re}(S^{xx}), \mathrm{Im}(S^{xx}), \mathrm{Re}(S^{xy}), \mathrm{Im}(S^{xy}), \mathrm{Re}(S^{yy}), \mathrm{Im}(S^{yy}), \mathrm{Re}(S^{yx}), \mathrm{Im}(S^{yx})$.

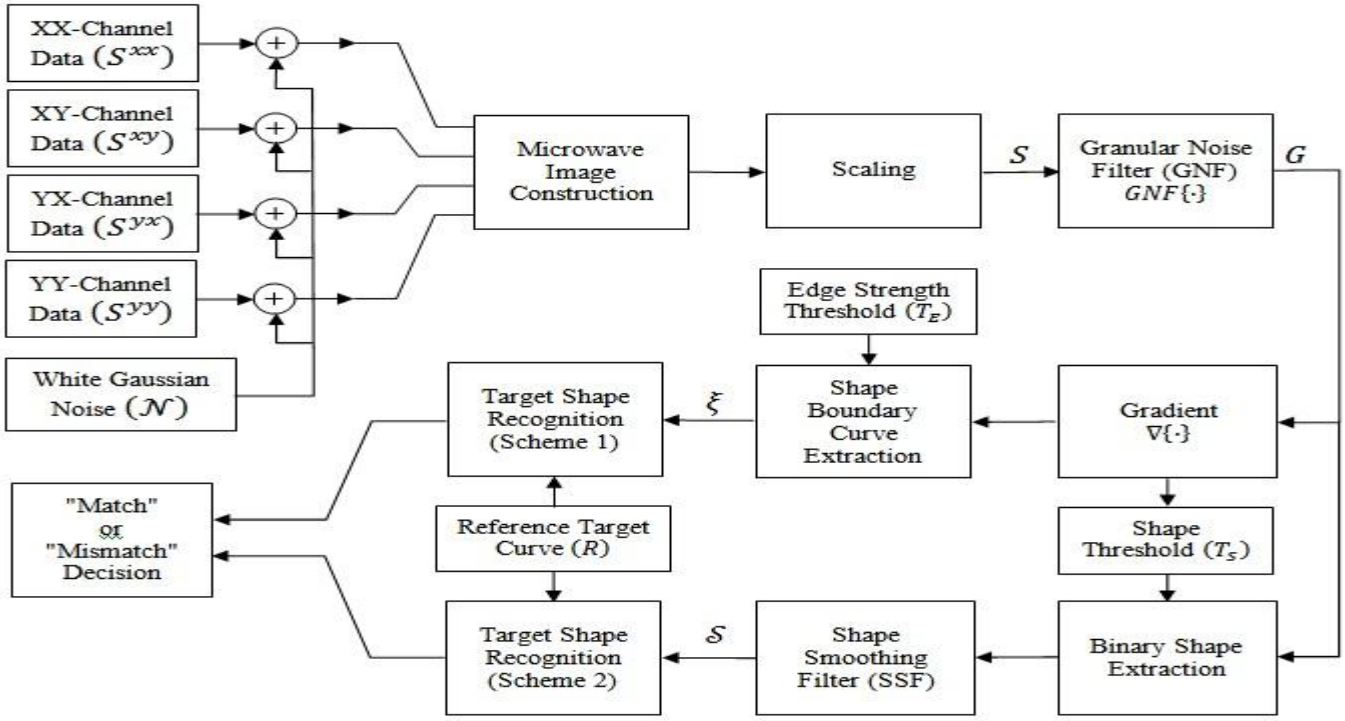

Figure 3: Block diagram showing GPR imaging and target shape recognition scheme

IV. EXTRACTION OF BURIED OBJECT SHAPE (BOS)

The value assigned to a given pixel(x, y) of the GPR image is compared to a predefined global threshold value T_S (the determination of which depends on the comparison with the images obtained for the same soil when there no target is present). If the value of a specific pixel exceeds the threshold value,T_S, it is considered that the pixel belongs to a buried object; otherwise it will be considered that the pixel belongs to the soil. In spite of being based on the above idea, it will be shown, in the following description, that the detection algorithm is cluster-based rather than pixel-based.

4.1. Application of Smoothing Shape Filter (SSF)

For avoiding false-alarm or erroneous target-missing while detecting a target of an arbitrary shape, the following cluster-based shape retrieving procedure is applied. Let a square window of size $W_S \times W_S$pixels be made in the GPR image and be centered at the pixel(x, y). Let the number of pixels belonging to this window and satisfying the condition $L > T_S$ be $n_b(x, y)$ and that the number of pixels satisfying the condition $L \leq T_S$be $n_s(x, y)$.

To scan the GPR image, the square window will slide over this image starting so that the upper-left corner of the window coincides with the upper-left pixel of the image and then moving towards right (i.e. on the image rows) pixel by pixel. When the upper-right corner of the sliding window reaches the right most pixel on the present row of the GPR image the window jumps to a new location so that its upper-left corner coincides with the left most pixel on the next row of the GPR image and then moving towards right again. This will be repeated until the GPR image is completely scanned and the decision is taken for all the image pixels. Following the above sliding window algorithm, a new image described by $n_b(x, y)$ is constructed; where x and y are the pixel coordinates in the new image (corresponding to the same coordinates in the original GPR image).

To get a two-dimensional drawing for the shape of the detected buried object, the following procedure is applied. For a window centered at the pixel(x, y): if $n_b(x, y) > n_s(x, y)$ a decision that the central pixel$(x, y)$of this widow belongs to a buried object should be taken; otherwise the decision will be that this pixel belongs to the soil. To construct a binary image showing the shape of the detected buried object one defines:

$$\mathcal{S}(x, y) = \begin{cases} 1, & n_b(x, y) > n_s(x, y) \\ 0, & n_b(x, y) \leq n_s(x, y) \end{cases} \tag{6}$$

An edge detection algorithm is then applied to the shape image, $\mathcal{S}(x, y)$, to get the shape boundary curve$\xi(x, y)$. This is described in detail in the next section.

V. EXTRACTION OF SHAPE BOUNDARY CURVE(SBC)

The Gradient Method is applied to the image$G(x,y)$ at the output of the GNF. A simplified one-dimensional method for edge detection is presented in Figure 4. The gradient of $G(x,y)$is a vector that can be calculated as follows:

$$\nabla G(x,y) = \begin{Bmatrix} Q_x \\ Q_y \end{Bmatrix} \tag{7}$$

Where,

$$Q_x = \frac{\partial G}{\partial x}, Q_y = \frac{\partial G}{\partial y} \tag{8}$$

The strength of the edge can be determined by the magnitude of the gradient

$$|\nabla G| = \sqrt{Q_x^2 + Q_y^2} \tag{9}$$

The direction of the gradient can be determined by the angle of the gradient

$$\angle \nabla G = \tan^{-1}\left(\frac{Q_y}{Q_x}\right) \tag{10}$$

The gradient can be approximated by finite differences as

$$Q_x = \frac{\partial G}{\partial x} = \frac{G(x+\Delta x, y) - G(x,y)}{\Delta x} \tag{11}$$

$$Q_y = \frac{\partial G}{\partial y} = \frac{G(x, y+\Delta y) - G(x,y)}{\Delta y} \tag{12}$$

Using pixel coordinate notaiton and setting $\Delta x = 1$ and $\Delta y = 1$ (*i.e.* one pixel)

$$Q_m \equiv Q_x = G(m+1, n) - G(m,n) \tag{13}$$

$$Q_n \equiv Q_y = G(m, n+1) - G(m,n) \tag{14}$$

The strength of the edge is expressed as

$$|\nabla G|_{m,n} = \sqrt{Q_m^2 + Q_n^2} \tag{15}$$

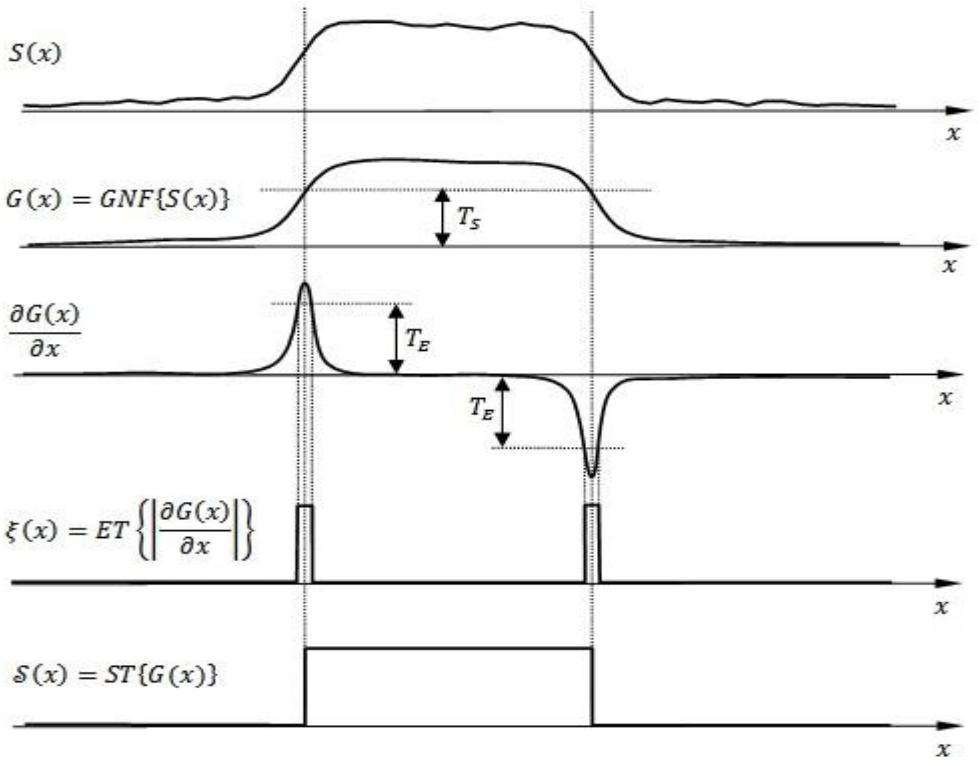

Figure 4: Simplified one-dimensional explanation of the edge detection technique used for extracting of the boundary curve of the buried object shape.

An edge strength threshold T_E is set to decide whether or not a pixel(m,n) belongs to an edge. If $|\nabla G|_{m,n} \geq T_E$ then the pixel(m,n) belongs to an edge otherwise it does not belong to any edge.

VI. TARGET SHAPE RECOGNITION

Given the retrieved SBC,$\xi(x,y)$, and the reference target boundary$R(x,y)$, a least-squared error method is applied to take the match or mismatch decision with a specific reference target shape. This method is described in thefollowing. Let $\xi(x,y)$ be designated as shape curve ξ and $R(x,y)$ be designated as the reference shape curve R. The shape curve ξ is translated so as to get its centroid coincident with the centroid of the reference shape curve R. The match or mismatch decision is taken based of the relative error defined as the ratio between the dashed area shown in Figure 5and the area enclosed by the boundary of the original target shape curve R.

$$\hat{e} = \frac{e}{A} \tag{16}$$

Where$e$ is the area subtended between the reference and retrieved curves (shown as dashed area in Fig. 5) and A is the area of enclosed by the reference curve.

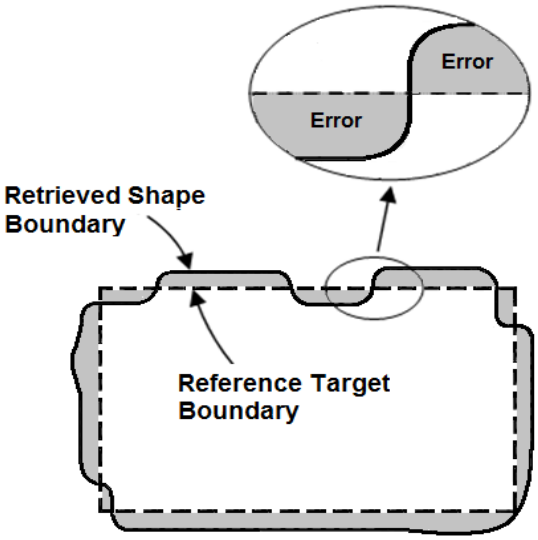

Figure5: Target shape recognition is achieved by comparing the retrieved shape to the original shape by subtracting the curvesξ and R for each corresponding pixel and summing the squared errors.

The polar coordinate system is used to allocate the corresponding points on both curves. The shape recognition process is applied by comparing the corresponding points on both curves. Referring to Figure 6, the differential area subtended between the differential element of the curve representing the retrieved shape and that of the curve representing the original target shape can be expressed as

$$\delta = \Delta_S \, d\varphi \tag{17}$$

Where,

$$\Delta_S = \frac{1}{2}[(r^S)^2 - (r^R)^2] \tag{18}$$

The absolute mismatch error can be expressed as

$$e = \int_0^{2\pi} |\Delta_S| d\varphi = \frac{1}{2}\int_0^{2\pi} |(r^S)^2 - (r^R)^2| d\varphi \tag{19}$$

The area of the original shape can be expressed as

$$A = \frac{1}{2}\int_0^{2\pi} (r^R)^2 \, d\varphi \tag{20}$$

By the aid of Figure 6, this squared error can be calculated numerical as follows.

$$e = \frac{\pi}{N}\sum_{n=1}^{N}[(r_n^S)^2 - (r_n^R)^2]^2 \tag{21}$$

Where$N$ is the number of angular segments to which the complete angle, 2π is divided as shown in Figure 7. The area enclosed by the reference (target) curve can be obtained as

$$A = \frac{\pi}{N}\sum_{n=1}^{N}(r_n^R)^2 \tag{22}$$

The relative error or shape mismatch can be expressed as

$$\hat{e} = \frac{e}{A} = \frac{\sum_{n=1}^{N}[(r_n^S)^2 - (r_n^R)^2]^2}{\sum_{n=1}^{N}(r_n^R)^2} \tag{23}$$

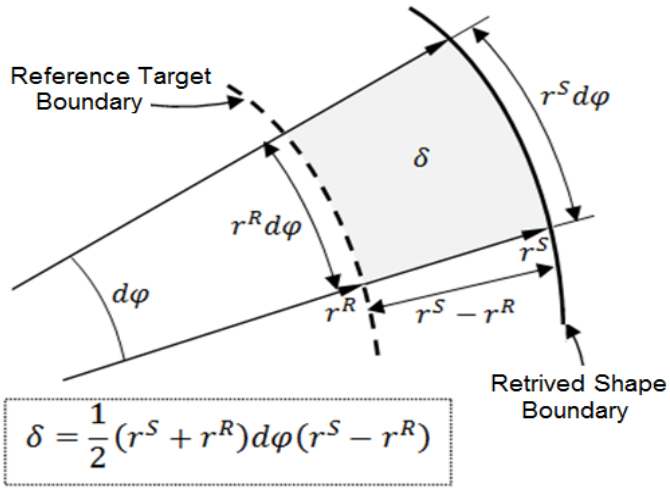

Figure6: Differential area subtended between the differential elements of the original and retrieved shape curves

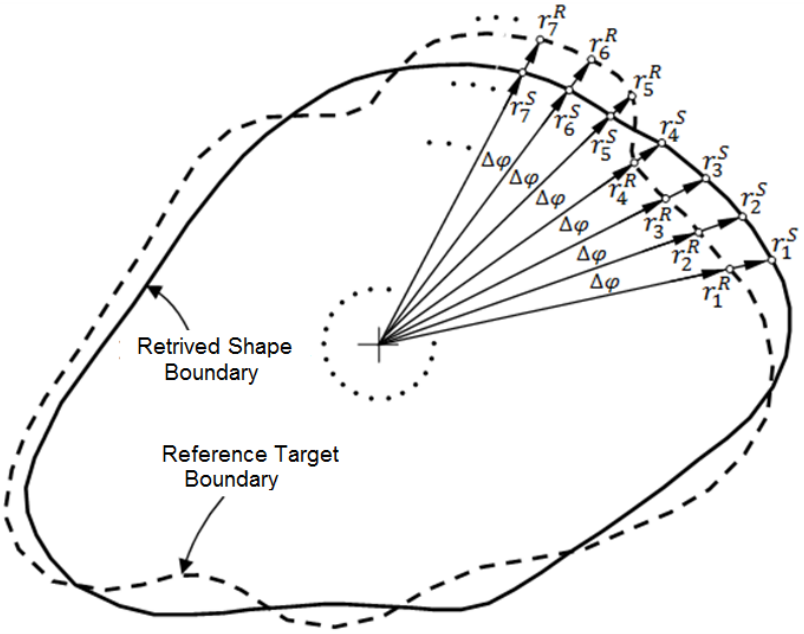

Figure 7: Target shape recognition is achieved by comparing the retrieved shape to the original shape by subtracting the curves S and R for each corresponding pixel and summing the squared errors.

VII. Noise Effect On The Shape Recognition Process

Considering a two-dimensional GPR image constructed according to the method described above, the value of the pixel$(m,n)$is determined by the coupling coefficient$S(m,n)$between the transmitting antenna and the receiving antenna on the m^{th} row and n^{th} column of the GPR antenna array.

$$S(m,n) = \frac{V_r(m,n)}{V_t} \tag{24}$$

Where$V_r(m,n)$is the complex voltage received by the antenna on the m^{th} row and n^{th} column of the GPR antenna array and$V_t$is the amplitude of transmitted sinusoidal voltage signal. Additive Gaussian noise causes the coupling coefficient to be modified as follows.

$$\acute{S}(m,n) = \frac{V_r(m,n) + \mathcal{N}(m,n)}{V_t} \tag{25}$$

Where$\mathcal{N}(m,n)$ is the value of the signal representing the noise picked by the same antenna. This noise is additive white Gaussian and causes a granular effect when viewing the GPR image as its value is randomly evaluated for each pixel.

$$\acute{S}(m,n) = S(m,n) + \frac{\mathcal{N}(m,n)}{V_t} \tag{26}$$

Equation (26) can be rewritten as

$$\acute{S}(m,n) = S(m,n) + \widehat{\mathcal{N}}(m,n) \tag{27}$$

Where$\widehat{\mathcal{N}}(m,n)$ is the value of the noise at the pixel(m,n)normalized to the amplitude of the transmitted voltage signal?

Equation (26) can be rewritten as

$$\acute{S}(m,n) = S(m,n)\left[1 + \left(\frac{V_r(m,n)}{\mathcal{N}(m,n)}\right)^{-1}\right] \tag{28}$$

The SNR at each pixel is defined as the ratio between the received signal power and the noise power at this pixel.

$$SNR(m,n) = \left|\frac{V_r(m,n)}{\mathcal{N}(m,n)}\right|^2 \tag{29}$$

Thus, the magnitude of the quantity $\left(\frac{V_r(m,n)}{\mathcal{N}(m,n)}\right)^{-1}$ appearing in (28) is inversely proportional to the square root of $SNR(m,n)$. It is clear from (28) that the lower the SNR, the more the deviation of $\acute{S}(m,n)$from$S(m,n)$, which means more distortion of the resulting GPR image.

VIII. GRANULAR NOISE FILTER (GNF)

For removing the granular noise effect appearing in the GPR image as described in section 7, the following filtering process to remove or reduce the noise "granules" from the GPR image is applied. Let a square window of size $W \times W$ pixels be made in the GPR image $\acute{S}(x,y)$and be centered at the pixel(x,y).

To scan the GPR image, the square window will slide over this image starting so that the upper-left corner of the window coincides with the upper-left pixel of the image and then moving towards right (i.e. on the image rows) pixel by pixel. When the upper-right corner of the sliding window reaches the right most pixel on the present row of the GPR image the window jumps to a new location so that its upper-left corner coincides with the left most pixel on the next row of the GPR image and then moving towards right again. This will be repeated until the GPR image is completely scanned pixel by pixel. At each position of the sliding window, the central pixel of the window is reassigned a new value calculated according to a weighted average as follows

$$p(x,y) = \frac{\sum_{i=1}^{W}\sum_{j=1}^{W} a_{i,j}\, p_0\left(x - \frac{W-1}{2} + i - 1, y - \frac{W-1}{2} + j - 1\right)}{\sum_{i=1}^{W}\sum_{j=1}^{W} a_{i,j}} \tag{30}$$

Where$p_0(x,y)$ is the original value of the pixel at the center of the sliding window and $p(x,y)$ is the newly calculated one; $a_{i,j}$ is the weights of the surrounding pixel values in the averaging process.

Following the above sliding window algorithm, a new image described by $G(x,y)$ is constructed; where x and y are the pixel coordinates in the new image corresponding to the same coordinates in the original GPR image, $\acute{S}(x,y)$.

IX. Results andDiscussion

In the following presentation and discussions, the two-dimensional complex polarimetric images are constructed from FDTD simulation where the operating frequency is 8 GHz. The cell size is 2×2×2 mm^3.Seven-cell PML is used to satisfy absorbing boundary condition. A GPR antenna array with one cluster and 54×54 crossed-dipole antenna elements is used. The dimensions of the antenna array are42.4cm×42.4cm and the length of the single dipole element is 6mm.The soil model represents red clay soil with 9.6% water content; which has the following electrical properties:$\varepsilon_r = 8.1, \mu_r = 1.0$, and $\sigma = 0.038$ S/m.

It should be noted that the soil type considered in the following investigations is polarization conservative and hence, the GPR data obtained from the co-polarization channels (*xx* and *yy*) are used for image construction, buried object shape extraction and target shape recognition.

9.1. Target Recognition under the Condition of High SNR

The GPR images areobtained for a metallic block of dimensions 14×14×7.2 cm buried at a depth of about 10 cm

below the ground surface using the polarimetric data given by equations (1)–(4). For visualizing the two-dimensional GPR data, the absolute value of the scattering parameters are shown in Figure8a for the *xx*-channel and Figure 8b for the *yy*-channel. Due to the high level of the SNR (30 dB), the granular effect is not clear in both figures. The image shown in Figure 8c is constructed from the *xx*-channel and *yy*-channel databy averaging the values corresponding to the each pixel in the two co-polarization channels. The image shown in Figure 8d is obtained by applying the GNF to the image shown in Figure 8c.

The procedure described in section 4 for BOS extraction is applied without using the SSF and the binary image described by equation (6) is then obtained and presented in Figure 8e. The SSF described in section 4is then applied to get the smoothed shape of the buried object shown in Figure 8f.

The procedure described in section 5 is applied to extract the SBC, which is presented in Figure 8g. For target shape recognition, the reference target shape and the retrieved SBC are compared with their centroids coincident with each other. The relative mismatch error between the two boundary-curves is then calculated using the expression given by (23). In this case the percentage mismatch error is 4.5%. Such small value of the relative mismatch error (less than 10%) means that the target is recognized.

9.2. Target Recognition under the Condition of Low SNR

The GPR images areobtained for the same block buried at the same depth. For visualizing the two-dimensional GPR data, the absolute value of the scattering parameters are shown in Figure 9a for the *xx*-channel and Figure 9b for the *yy*-channel. Due to the low level of the SNR (5 dB), the granular effect is clear in both figures. The image shown in Figure 9c is constructed from the *xx*-channel and *yy*-channel data by averaging the values corresponding to the each pixel in the two co-polarization channels. The image shown in Figure 9d is obtained by applying the GNF to the image shown in Figure 9c. It is clear, by comparing Figures 9c and 9d, that the granular noise is considerably reduced due to the application of the GNF.

The procedure described for BOS extraction is then applied without the SSF and the binary image is then obtained and presented in Figure 9e. The SSF is then applied to get the smoothed shape of the buried object shown in Figure 9f.

The procedure described in section 5 is applied to extract the SBC presented in Figure9g. For target shape recognition, the reference target shape and the retrieved SBC are compared with their centroids coincident with each other. The relative mismatch error between the two boundary-curves calculated in this case is 9.5%. The error is increased in comparison with the last case due to the increased noise level. However, the value of the relative mismatch error is still less than 10%, which means that the target is recognized. This reflects the efficiency of the applied technique which leads to successful recovery of the buried object shape even in the case of low SNR.

9.3. Effect of the SNR on the Buried Target Shape Recognition Process

The GPR images and the retrieved SBC obtained for a metallic block of dimensions 14×14×7.2 cm buried at a depth of about 10 cm below the ground surface are shown in Figure 10 for different values of the SNR ranging from 30 dB to 0 dB.The relative mismatch error resulting from the comparison between the reference target shape and the retrieved SBC for each value of the SNR is shown on the right-most column of Figure 10.It is clear that, with reducing the SNR, the relative mismatch error increases leading to erroneous missed-target decision for SNR≤3 dB for this target.

The GPR imagesand the retrieved SBC obtained for a metallic cylinder of 7 cm radius and 7.2 cm height buried at a depth of about 10 cm below the ground surface are shown in Figure 11 for different values of the SNR ranging from 30 dB to 0 dB. The relative mismatch error resulting from the comparison between the reference target shape and the retrieved SBC for each value of the SNR is shown on the right-most column of Figure 11. It is clear that, with reducing the SNR, the relative mismatch error increases leading to erroneous missed-target decision for SNR≤4 dB for this target.

9.4. Reduction of the Noise Effect due to the Application of the GNF

The application of the GNF on the GPR image constructed from the four polarimetricchannels data has the effect of considerable reduction of the relative mismatch error especially at the low values of SNR.

For a metallic block of dimensions 14×14×7.2 cm buried at a depth of about 10 cm below the ground surfacea plot for the relative mismatch error against the SNR is shown in Figure 12. It is shown that the application of the GNF results in the possibility of correct decision for target shape recognition even at SNR of 3 dB.

For a metallic cylinder of 7 cm radius and 7.2 cm height buried at a depth of about 10 cm below the ground surface a plot for the relative mismatch error against the SNR is shown in Figure 13. It is shown that the application of the GNF results in the possibility of correct decision for target shape recognition even at SNR of 4 dB.

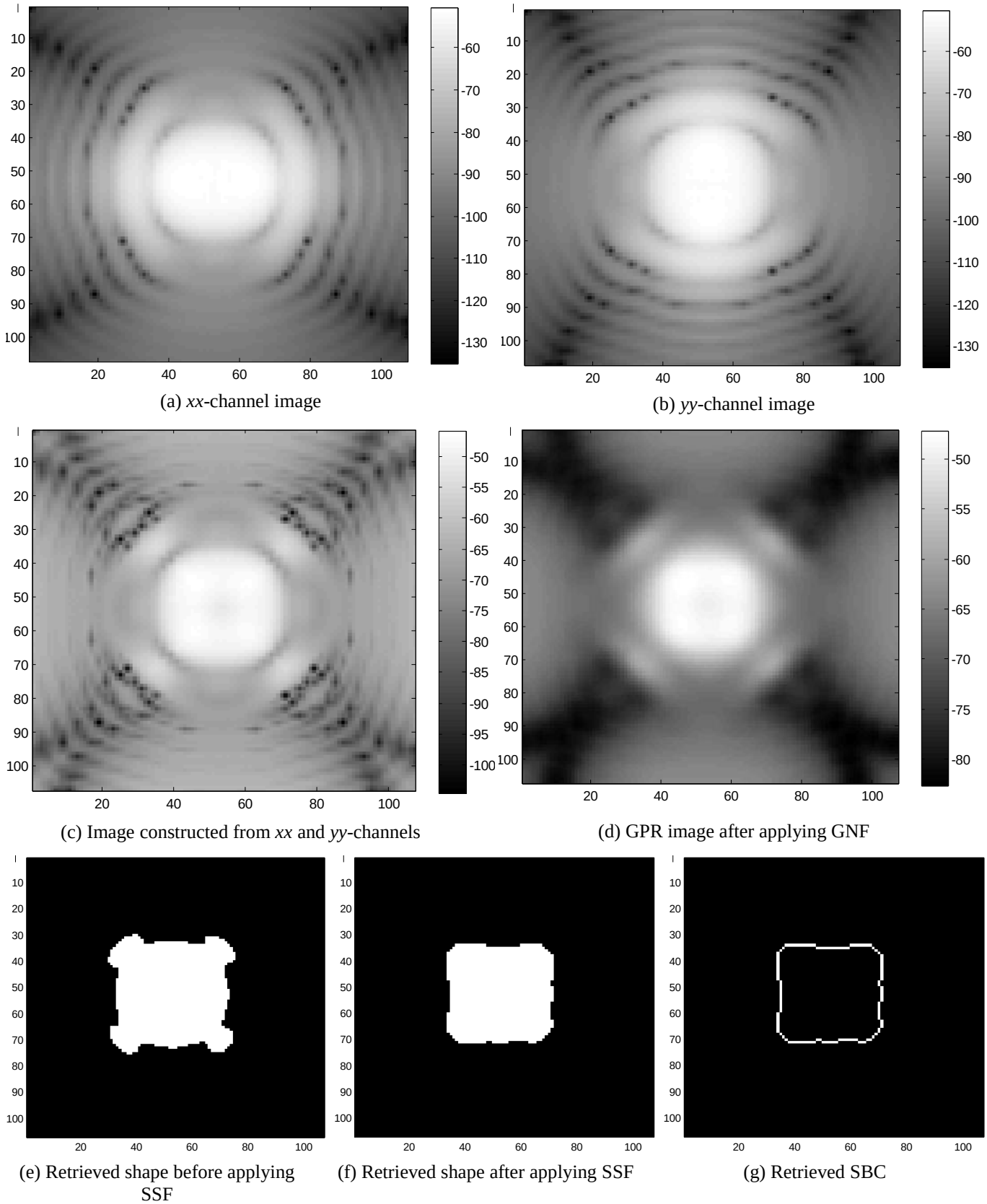

(a) *xx*-channel image

(b) *yy*-channel image

(c) Image constructed from *xx* and *yy*-channels

(d) GPR image after applying GNF

(e) Retrieved shape before applying SSF

(f) Retrieved shape after applying SSF

(g) Retrieved SBC

Figure 8:The process of retrieving boundary curve for the buried object under high SNR for a metallic box of dimensions 14×14×7.2 cm buried at a depth of about 10 cm below the ground surface using the proposed GPR system(SNR=30dB) (Mismatch error = 4.5%)

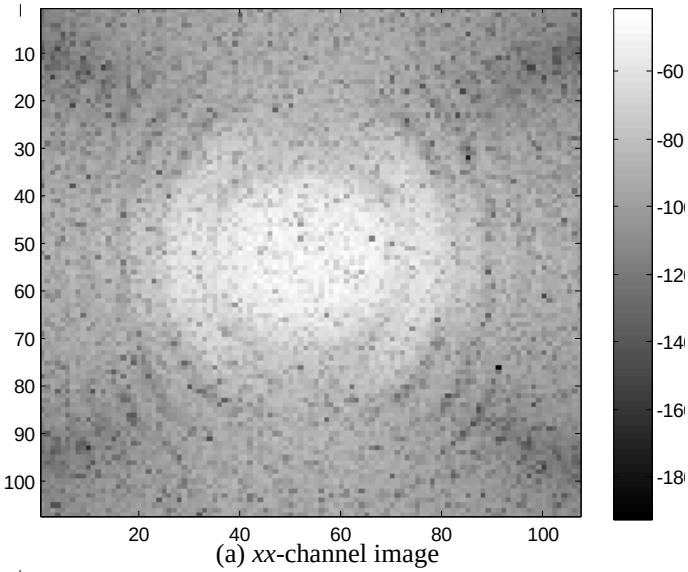

(a) *xx*-channel image

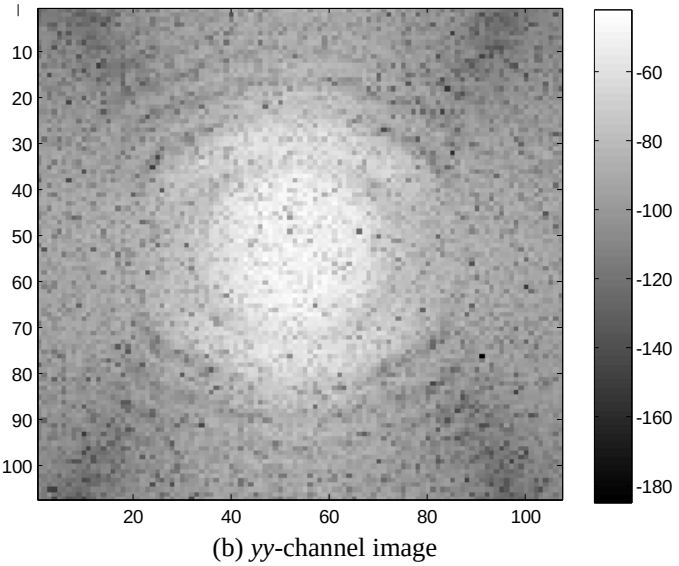

(b) *yy*-channel image

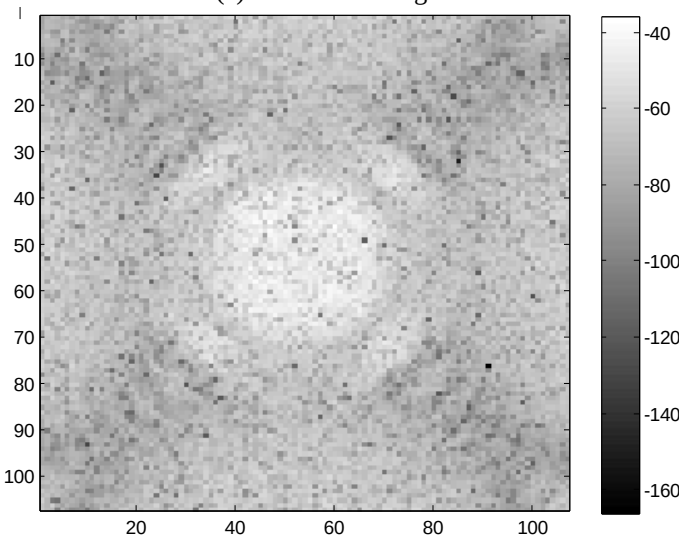

(c) Image Constructed from *xx* and *yy*-channels

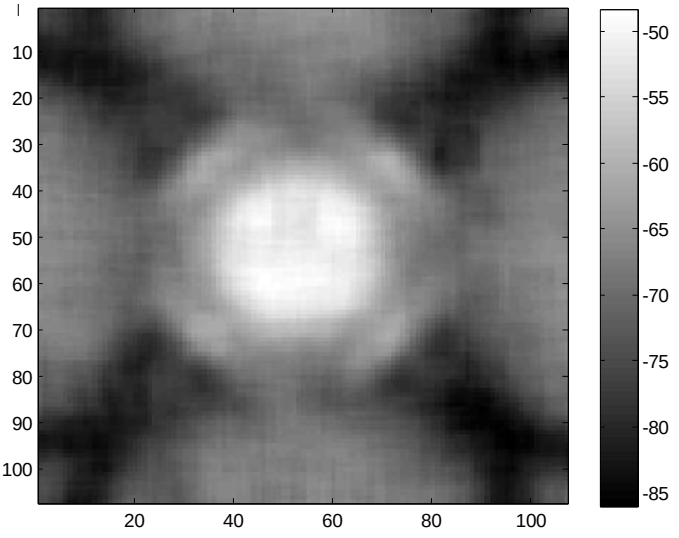

(d) GPR image after applying GNF

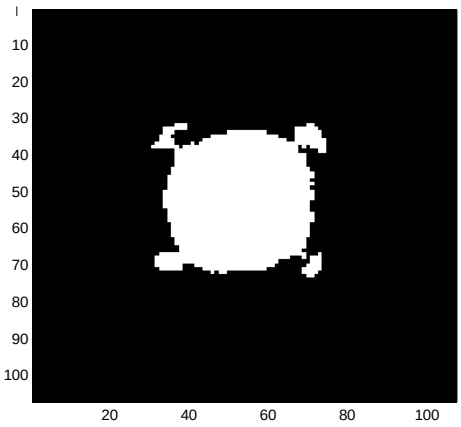

(e) Retrieved shape before applying SSF

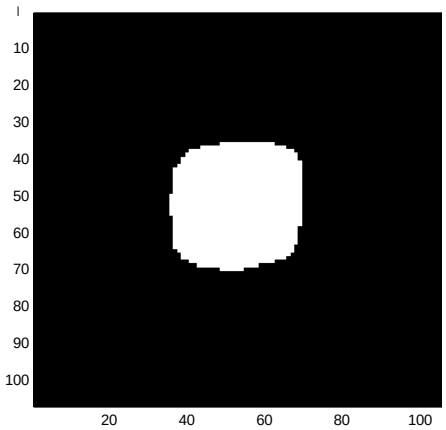

(f) Retrieved shape after applying SSF

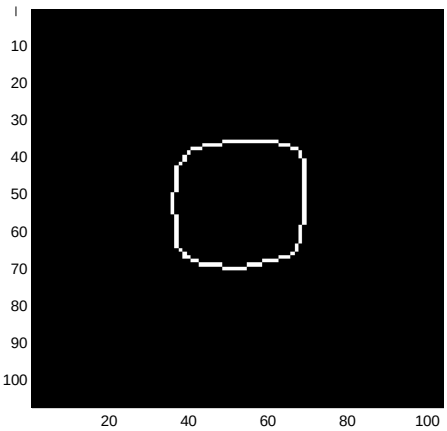

(g) Retrieved SBC

Figure 9: The process of retrieving boundary curve for the buried object under low SNR for a metallic box of dimensions 14×14×7.2 cm buried at a depth of about 10 cm below the ground surface using the proposed GPR system (SNR=5dB) (Mismatch error = 9.5%)

SNR (dB)	GPR Image	GNF Image	Extracted SBC	%Error
30	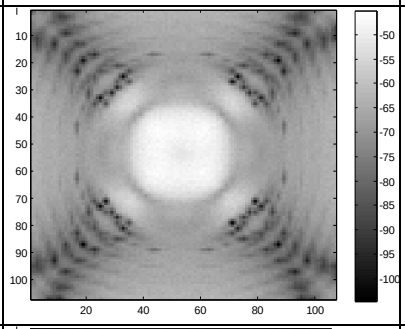	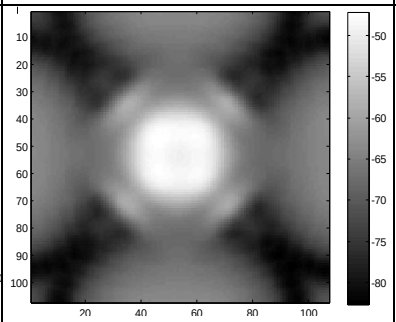	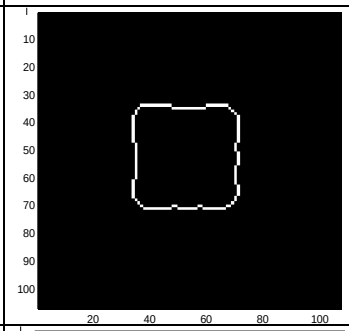	7%
15	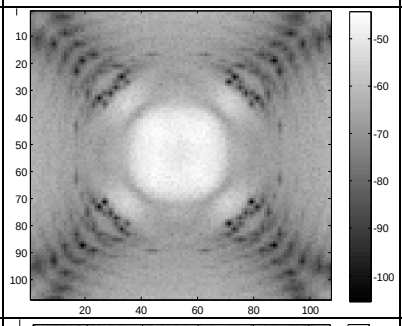	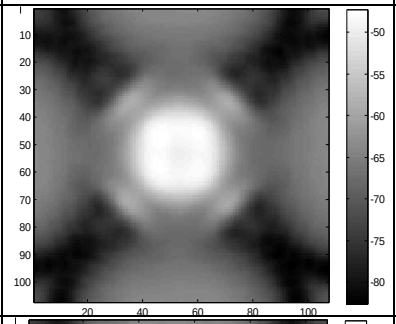	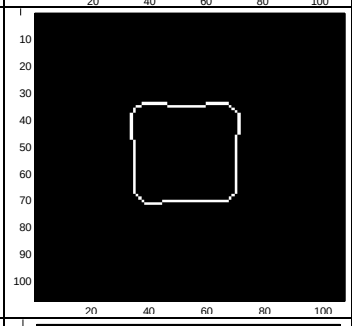	8%
10	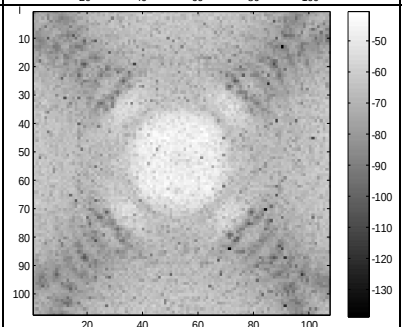	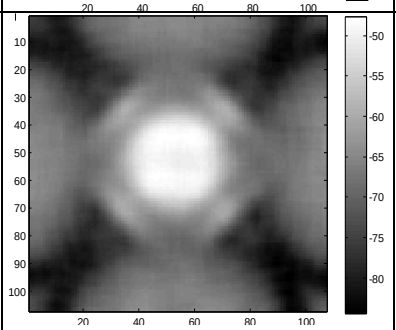	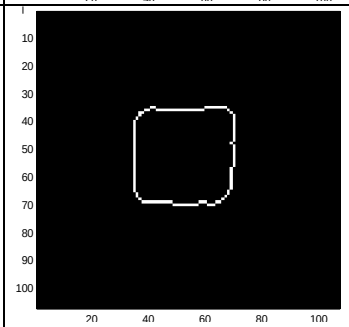	9%
1	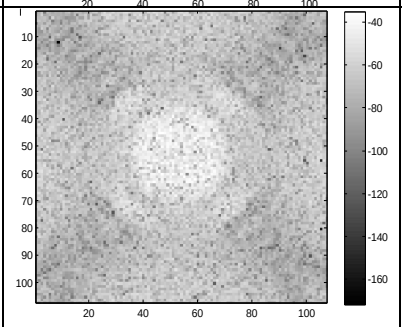	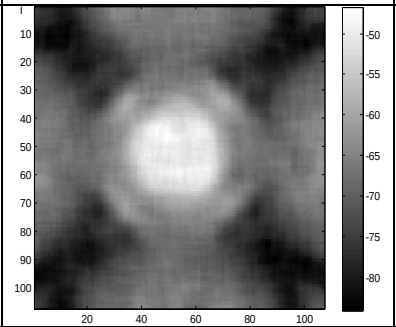	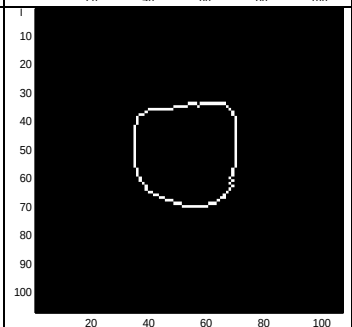	19%
0	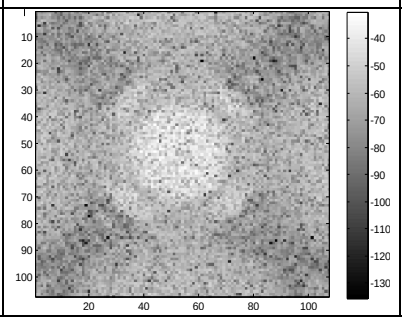	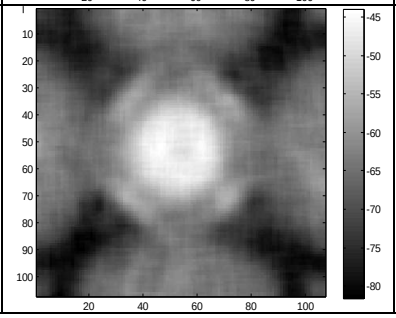	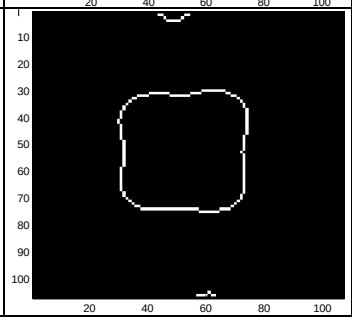	34%

Figure 10: Effect of the SNR ratio on the GPR image and the resulting mismatch error between the retrieved SBC and the reference target shapefor a metallic box of dimensions 14×14×7.2 cm buried at a depth of about 10 cm below the ground surface using the proposed GPR system

SNR (dB)	GPR Image	GNF Image	Extracted SBC	%Error
30	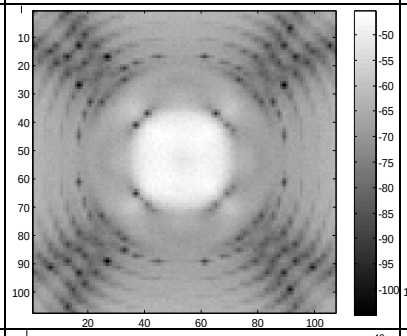	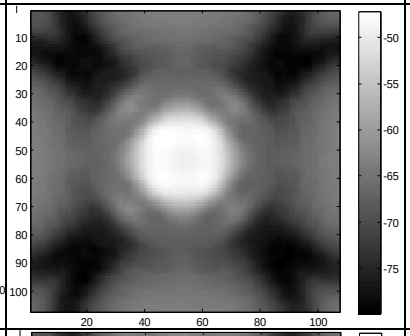	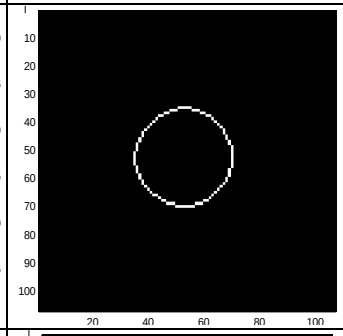	3%
15	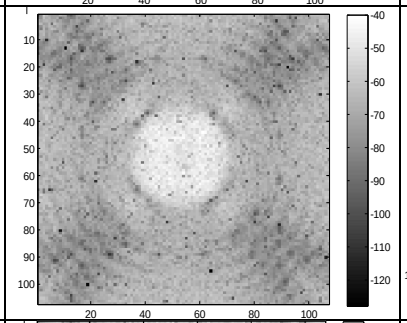	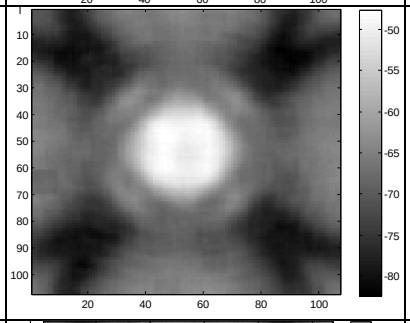	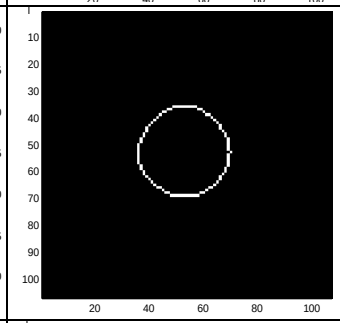	4%
10	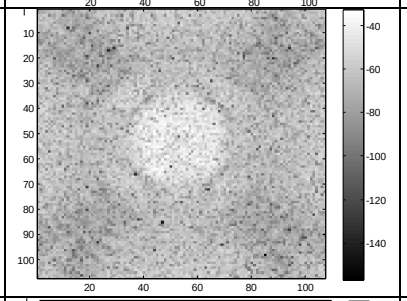	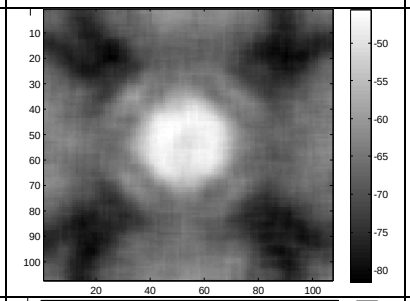	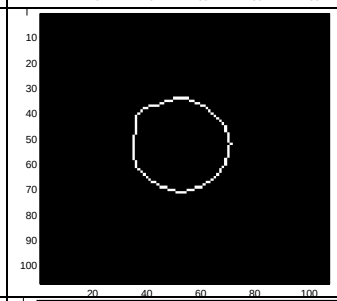	4.5%
3	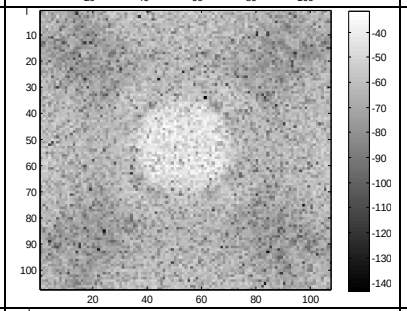	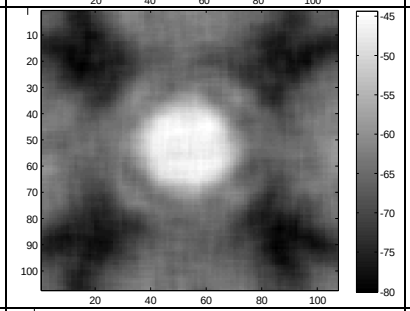	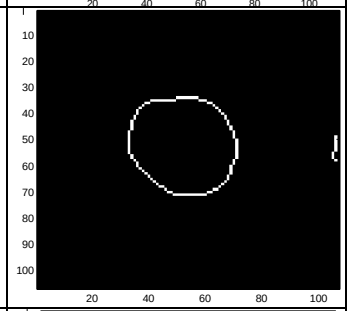	12%
0	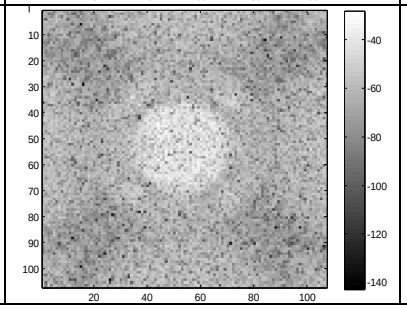	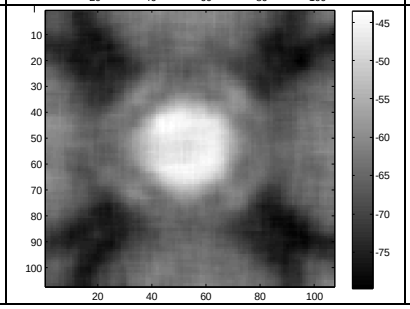	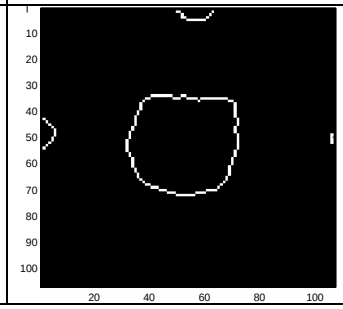	35%

Figure 11: Effect of the SNR ratio on the GPR image and the resulting mismatch error between the retrieved SBC and the reference target shape for a metallic cylinder of 7 cm radius and 7.2 cm height buried at a depth of about 10 cm below the ground surface using the proposed GPR system

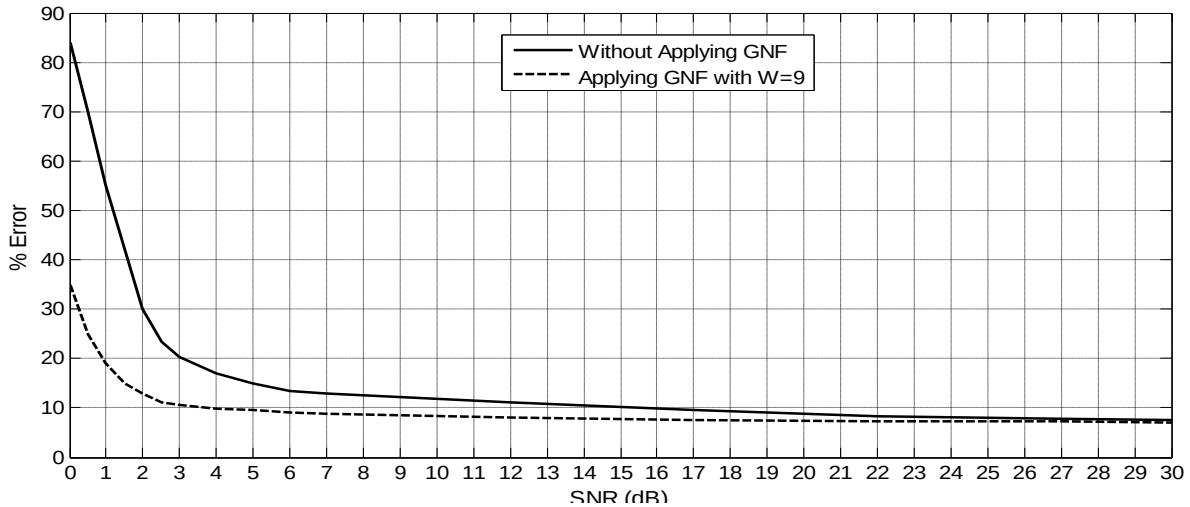

Figure 12: Reduction of the resulting error in target shape recognition algorithm due to the application of granular noise filter for a metallic box of dimensions 14×14×7.2 cm buried at a depth of about 10 cm below the ground surface using the proposed GPR system.

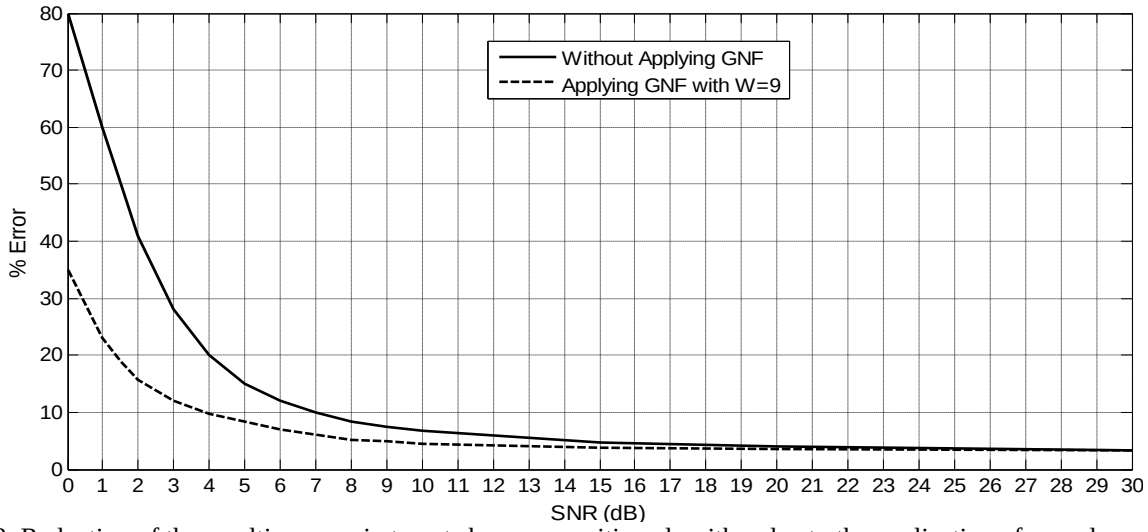

Figure 13: Reduction of the resulting error in target shape recognition algorithm due to the application of granular noise filter for a metallic cylinder of 7 cm radius and 7.2 cm height buried at a depth of about 10 cm below the ground surface using the proposed GPR system

X. CONCLUSION

An efficient technique for the treatment of buried object shape recognition from noisy polarimetric GPR images is introduced. The GPR system used for obtaining high resolution polarimetric images for objects buried under the surface of a ground soil together with the object shape retrieval and target recognition are completely described. A GNF is introduced to get an image with increased SNR. An algorithm to extract a two-dimensional shape of the buried object is introduced. An SSF is then applied for further elimination of the errors resulting due to granular noise effect on the two-dimensional shape retrieval process.A shape recognition algorithm is applied to compare the retrieved shape for the buried object to a reference target shapeto take a match or mismatch decision. The proposed GPR antenna system and the suggested algorithms for noise reduction, shape extraction and target recognition are examined through FDTD simulation running on different buried target shapes. The numerically obtained results show that proposed noise reduction technique with the proposed GPR system and the suggested algorithms for shape extraction and target shape recognition are efficient and successful in all the examined cases.

REFERENCES

[1] Y. Jeng, Y. Li, C. Chen, H. Chien, "Adaptive filtering of random noise in near-surface seismic and ground-penetrating radar data", Journal of Applied Geophysics No. 68, pp. 36–46, 2009.

[2] L. Crocco and F. Soldovieri, "Bistatic tomographic GPR imaging for incipient pipeline leakage evaluation", Progress In Electromagnetics Research, PIER 101, pp. 307-321, 2010.

[3] R. Roberts, D. Cist, and A. Kathage, "Full-resolution GPR imaging applied to utility surveying: insights from multi-polarization data obtained over a test pit", IWAGPR 2009, 5th International Workshop on GPR, Granada, Spain, May 27-29, 2009.

[4] J. Groenenboom and A. Yarovoy, " Data Processing and Imaging in GPR System Dedicated for Landmine Detection", Subsurface Sensing Technologies and Applications, Vol. 3, No. 4, pp 387-402, Oct. 2002.

[5] L. Morrow and P.Genderen, "2D polarimetricbackpropagation algorithm for ground-penetrating radar applications", Microwave and Optical Technology Letters, Vol. 28, pp. 1–4, 2001

[6] K. Dongen, P. Berg, and J.Fokkema, "Adirectional borehole radar for three-dimensional imaging", Proceedings of the 9thInternationalConf. GPR I,pp. 25–30, 2002.

[7] I. Catapano, F. Soldovieri, and L. Crocco, "On the feasibility of the linear sampling method for 3D GPR surveys," Progress In Electromagnetics Research, Vol. 118, 185-203, 2011.

[8] Y. Huang, Y. Liu, Q. H. Liu, and J. Zhang, "Improved 3-d GPR detection by NUFFT combined with MPD method," Progress In Electromagnetics Research, Vol. 103, 185-199, 2010.

[9] G. E. Atteia and K. F. A. Hussein, "Realistic model of dispersive soils using PLRC-FDTD with applications to GPR systems," Progress In Electromagnetics Research B, Vol. 26, 335-359, 2010.

[10] C.Ozdemir, S. Lim and H. Ling, "A synthetic aperture algorithm for ground-penetrating-radar imaging", Microwave and Optical Technology Letters, Vol. 42, pp. 412-414, 2004.

[11] K. M. Ibrahim, K. F. A. Hussein and A. A.Ammar, " Two-dimensional imaging and shape recognition of land buried objects through polarimetric ground penetrating radar", The 2nd Middle East Conference on Antennas and Propagation“ MECAP” 2012 in Cairo, Egypt, December 2012.